Analysis of the Expected Thrust Misalignment of Kaufman Thrusters

R. L. SELIGER,* G. R. NUDD,* G. R. BREWER,† AND K. AMBOSS‡
Hughes Research Laboratories, Malibu, Calif.

In the design of a spacecraft using solar powered electric propulsion, it is important to know accurately the expected misalignment of the thrust vector from the thruster, so that the misalignment can be adequately compensated. This paper reports the results of an analytical study to determine the causes and magnitudes of thrust misalignment from a Kaufman-type electron bombardment ion thruster. The effect of perturbations in the spacing and transverse alignment of the accelerating electrodes on the ion beam direction and magnitude was determined by means of a digital computer program. This analysis included the detailed changes in plasma sheath position which accompany electrode shifts and changes in current. Expected electrode distortion due to thermally induced stresses was calculated. Since the perturbations considered are small, it is valid to assume that the thrust variations are linear over the range. The results are therefore presented in terms of linear coefficients from which the expected thrust vector change can be determined. The effect of electrode misalignment is found to be most significant in high perveance flow; for instance the rate of change of axial thrust with axial electrode spacing at 3.4×10^{-6} electron pervs is 1.63×10^{-7} lb/mil, while at 0.985×10^{-6} electron pervs it decreases to 0.33×10^{-7} lb/mil.

Introduction

As a result of comprehensive studies over the past several years, the fundamental design concepts associated with solar powered electric propulsion systems for interplanetary missions have become fairly well defined. For example, it is known that the engine array will involve a cluster of thruster modules which may be arranged on a frame that can be translated in two directions (or other suitable motion) relative to the spacecraft. This translational motion is necessary in order to assure that the center of thrust will pass through the center of mass of the spacecraft, for any configuration of active and inactive thrusters. In addition to changes in the thrust axis due to switching of thrusters, the vector from an individual thruster will not necessarily be along the axis and could change slightly in magnitude and direction with time or as a result of changes in thruster operating parameters. The effect of these misaligned thrust vector components around the pitch and yaw axes can be negated by the translation mechanism mentioned above. The component around the roll axis, however, can be compensated only by the spacecraft attitude control system or by gimballing some or all of the thrusters. As an indication of the seriousness of the thrust misalignment problem, it can be shown easily that a misalignment angle of 0.1 rad between the thrust axis and the motion axis of an interplanetary spacecraft will require several hundreds of pounds of propellant by a corrective chemical attitude control system for a 250 day mission. It is seen that this additional weight is comparable to a typical payload and cannot be ignored. Therefore, it is of considerable importance to SEP spacecraft design to know the expected thrust vector misalignment as a function of various thruster operational parameters, mechanical displacements, and time. Such knowledge is also fundamental to the development of techniques of thruster construction for reducing the changes in the thrust vector.

The thruster analyzed herein is a standard electron bombardment type with screen and accelerator electrodes, each containing an array of circular apertures through which the ion beamlets are extracted. These apertures are aligned in the two electrodes during electrode fabrication and upon thruster assembly. The screen electrode apertures are countersunk on the plasma side. A drawing of the thruster showing an enlargement of the aperture chosen for study is shown in Fig. 1.

In a study reported previously, Lathem[1] analyzed the effects of transverse electrode misalignment on the ion trajectories of a SERT II-type electron bombardment thruster. The present paper supplements this previous work by 1) including the effect of change in the shape of the plasma sheath ion source as the electrodes are moved transversely (Lathem assumed a fixed shape for all perturbed geometries); 2) including the effects of spacing change between electrodes; and 3) analyzing the magnitude of electrode distortion caused by thermal stresses. The results of this work are compared with those of Lathem where applicable.

Pertinent Thruster Parameter Changes

A number of operational and dimensional parameters of the electron bombardment thruster may vary during assembly, launch, or normal operation and can change the thrust vector of an array of such thrusters. Those parameter changes that are important to consider include: 1) transverse displacement of the accel electrode relative to the screen electrode in assembly of the thruster or due to vibration on launch; 2) changes in the current of the thruster due to a) a change in spacing between accel and screen electrodes caused by thermal buckling, or b) change in propellant flow rate; 3) change in alignment between accel and screen apertures due to relative radial thermal expansion.

As illustrated in Fig. 1, under ideal conditions the electrodes of an electron bombardment thruster may be described as an array of aligned circular apertures. The main thrust axis is defined by the large cylindrical discharge chamber with the circular parallel electrodes in planes perpendicular to it at one end. Several thousand hole pairs in the electrodes,

Presented as Paper 69-303 at the AIAA 7th Electric Propulsion Conference, Williamsburg, Va., March 3–5, 1969; submitted April 18, 1969; revision received October 9, 1969. This work was supported by Jet Propulsion Laboratory.

* Member of the Technical Staff, Ion Physics Department.
† Manager, Ion Physics Department. Member AIAA.
‡ Consultant, Electron and Ion Beam Technology, Malibu, Calif.

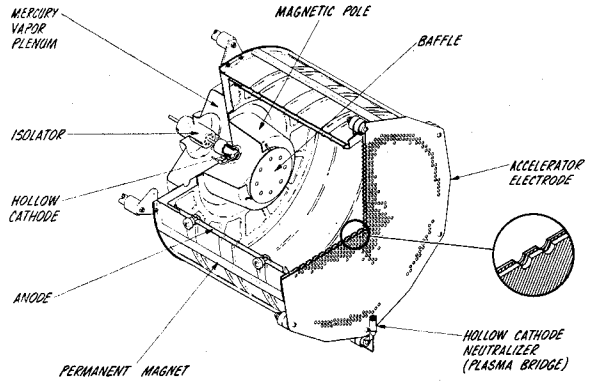

Fig. 1 Low specific impulse mercury ion thruster.

located symmetrically about the thrust axis, form an array of small cylindrical accelerating structures whose axes are ideally all aligned parallel to the thrust axis. If the ion density in the discharge chamber is not axisymmetric, or if any of the aligned cylindrical accelerator apertures become misaligned, perturbations in the thrust vector will be incurred.

Of the many possible causes of thrust vector perturbation it is reasonable to study in most detail those that are most likely to occur and that produce the largest thrust disturbances. Although some mechanical features of the electron bombardment thruster, such as discharge chamber layout or the form of the electrode support structure, could lead to thrust vector perturbations (due to nonsymmetric discharge profiles or motions of the electrodes), it is believed these design features are amenable to changes as required to improve the symmetry and so reduce the thrust vector change. On the other hand, the thermal buckling of the electrodes is a problem that is fundamental to the contemporary method of constructing the accelerator system, and this buckling can produce serious changes in the thrust vector. This aspect of the problem was, therefore, studied in more detail. The most serious motion of the electrodes is axial displacement or bowing caused by thermal stresses. Because of the seriousness of the buckling problem in operating thrusters, electrodes are usually given an initial bow so that the direction of subsequent motion can be made to be the same as that of the two plates. It will be shown that a spacing change in prebowed plates can occur from a uniform 0.090 in. to a parabolic distribution, which varies from 0.090 in. at the edge to 0.045 in. at the center; this will cause a significant change in thrust magnitude.

A number of forms of apertures misalignments can result from electrode buckling or in assembly; these are illustrated in Fig. 2. Figure 2a shows the unperturbed geometry; in Fig. 2b the electrode spacing is decreased while the rotational symmetry of the apertures is preserved; this change results in an increase in the magnitude of the thrust from this aperture. In Fig. 2c, the electrodes are displaced normal to the beam axis, thus destroying its symmetry and causing a

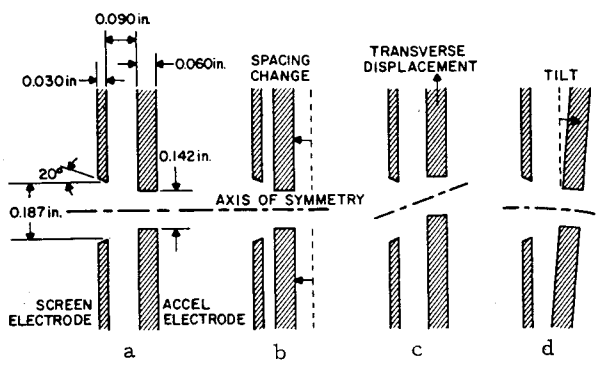

Fig. 2 Basic electrode misalignments.

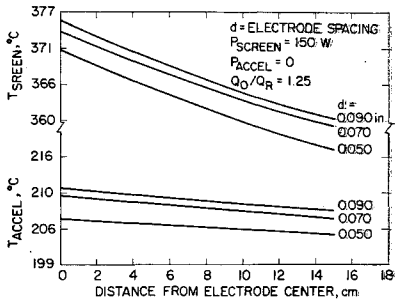

Fig. 3 Dependence of grid system temperature distributions on electrode spacing.

change in the magnitude and direction of the thrust vector. The case illustrated in Fig. 2d involves a tilt in one electrode with respect to the other.

Although changes in electrode spacing are the only cause of misalignment which have been predicted analytically, the thrust vector perturbations caused by a number of other modes of electrode misalignment have been evaluated. The results of the thermal buckling analysis are presented in two main parts: 1) the thermal analysis leading to the grid system temperature distributions, and 2) the stress analysis of the mechanically loaded electrodes with given temperature distribution.

Thermal Analysis

In order to find the thermal distortion in the electrode system, it was first necessary to determine the steady-state temperature distribution. From experimental measurements on a thermal mockup of a bombardment thruster, it was concluded that a large number of multiple reflections occur inside the discharge chamber, in such a way that the heat flux distribution is fairly uniform across the screen electrode. Therefore, the thermal analysis was directed toward a detailed simulation of the electrode system, assuming various incident heat flux distributions from the discharge chamber.

The multiple reflection heat transfer in the electrodes was simulated by a thermal analysis computer program. A parametric study of the equilibrium electrode system temperature distribution was made for the electrode geometry (see Table 1). Studies were made of the sensitivity of the electrode temperature distributions to variations in a) electrode spacing, b) discharge power distribution, c) total discharge power, and d) interception power.

The six curves in Fig. 3 give the screen and accelerator electrode temperature distribution for three values of electrode spacing and for an assumed incident heat flux that decreases linearly from value Q_0 at the center to Q_R at the edge. As shown, decreasing the interelectrode spacing lowers the over-all temperatures of both electrodes. The grid system appears more transparent to the incident radiation as the electrode spacing decreases.

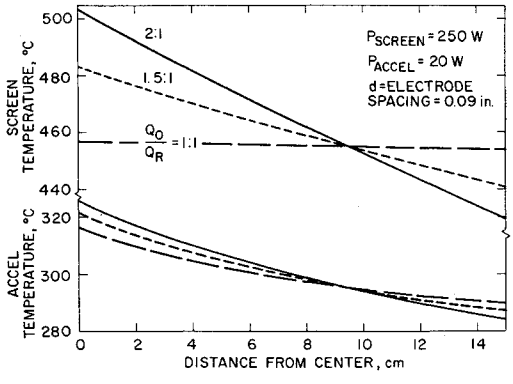

Fig. 4 Dependence of electrode temperatures on discharge power distribution.

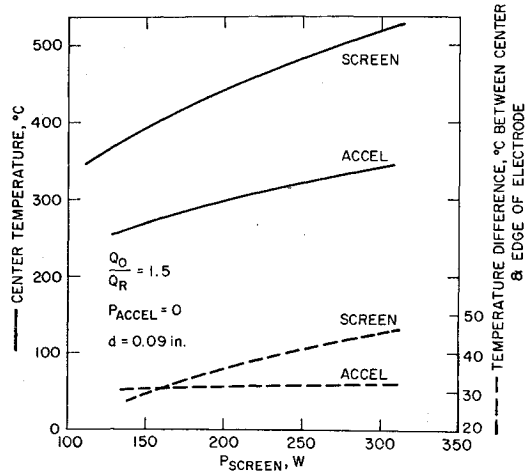

Fig. 5 Dependence of electrode temperatures on power incident on screen P_{screen}.

The heat flux distribution from the discharge chamber was assumed to vary in these calculations. Since heat conduction is small in the screen electrode (because it is thin and highly perforated), its temperature gradient from center to edge will depend strongly on the ratio Q_0/Q_R. This dependence is illustrated by the three sets of temperature distributions in Fig. 4, which correspond to Q_0/Q_R = 1, 1.5, and 2. For all three cases the total discharge power incident on the screen is 250 w and the interception power into the accelerator is 20 w. The heat intensity ratio Q_0/Q_R = 1.5 gives rise to a 40°C temperature variation from the screen center to edge. This value is considered reasonable and is used in the subsequent sensitivity studies.

The total heat flux incident on the screen electrode P_{screen} from the discharge chamber is highly dependent on the specific discharge chamber performance characteristics (e.g., the ionization efficiency) and the operating point of the thruster. The variations in the screen and accelerator center temperatures and center-to-edge temperature differences have thus been calculated as functions of the total discharge power. The curves are shown in Fig. 5.

As illustrated in Figs. 4 and 5, the effects of varying the discharge power intensity ratio Q_0/Q_R and the total discharge power are most noticeable on the screen electrode. Another source of power into the grid system is the heating of the accelerator by intercepted ions (P_{accel}), which may be produced by charge exchange collisions. Relatively small amounts (10–20 w) of interception power cause noticeable accelerator temperature changes, as shown in Fig. 6. The accelerator center-to-edge temperature difference is increased from 10°C to 30°C by 20 w of interception power.

A thermal model of the electrode system is described previously for predicting the temperature distribution of the electrodes under normal operating conditions. Since the current practice is to align the electrodes precisely during assembly at room temperature, the difference between the electrode operating temperatures and room temperature may cause stress producing thermal gradients in the electrodes. It is believed that the stresses produced as the electrode system undergoes heating to operating temperature produce the largest axisymmetric misalignments that are likely to occur. Therefore, a significant effort was devoted to predicting these misalignments quantitatively. The natural extension of this analysis is misalignments resulting from nonaxisymmetric thermal stresses, which is of concern for operating thrusters in an array.

Stress Analysis

A computer program that analyzes shells by the finite element method was used to study the thermal-buckling of the electrodes. The computer program can handle shells of revolution subject to axisymmetric or asymmetric mechanical and thermal loads. In this calculation, an electrode is divided into washer shaped regions that form the elements of the model. Thermal and mechanical loads are prescribed on each element and the computer program solves the equations of motions for the deformations. Since the dimensions of each element can be specified independently, initially dished electrodes can be considered. Because the stress analysis program considers solid plates, an equivalent set of thermal and elastic parameters was used in the solid plate analysis in order to simulate the actual punched plate electrode. The relationships between the perforated and unperforated values of Young's moduls and Poisson's ratio were obtained from a paper by O'Donnell and Langer.[2]

Thermal warping of the screen and accelerator electrodes was first calculated for a representative temperature distribution which corresponds to an incident screen power of 200 w, with Q_0/Q_R = 1.5 and 20 w of interception power (case 1 of Fig. 6). The radial and axial displacements of the electrodes are shown in Fig. 7. Both electrodes were initially dished to a depth of 0.010 in. and no mechanical loading is present under those conditions. The small perturbations in alignment which occur are 1) a decrease in electrode spacing of 0.003 in. maximum at the center and 2) radially outward differential motion of the screen holes with respect to the accelerator holes, with the maximum 0.0044 in. at the edge. Some indication of the behavior of a grid system (initially aligned at room temperature) when heated to operating temperature can be derived from this warping calculation.

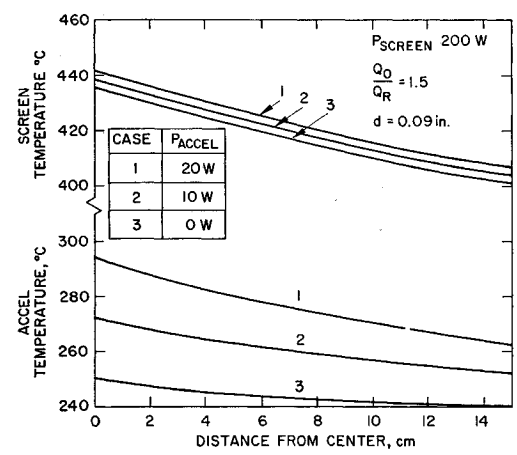

Fig. 6 Dependence of electrode temperatures on interception power.

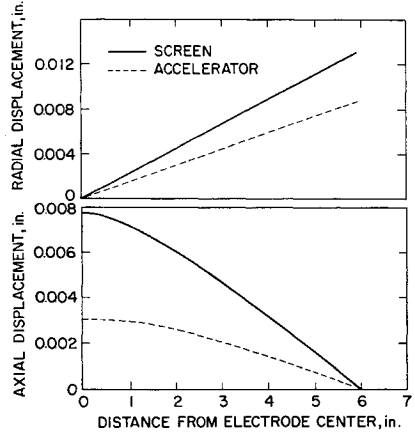

Fig. 7 Axial and radial displacement of electrodes due to thermal warping with no mechanical loading.

The main effects are: 1) radial and axial displacements of both electrodes will occur; 2) both displacements will be greater for the screen because it becomes hotter with a larger temperature gradient, has a larger open area, and is thinner than the accelerator electrode; 3) the misalignments which result from the above displacements are a) a decrease in the electrode spacing, and b) a transverse (radially outward) motion of the screen holes with respect to the accelerator holes; 4) the magnitude of the decrease in spacing resulting from bowing of both electrodes is most dependent on the temperature gradients; the magnitudes of the radial displacements depend on the over-all temperature levels of the electrodes.

These warping calculations revealed the main buckling motions found in the electrode system. It was found also that the magnitudes of these motions are highly sensitive to the mechanical design of the electrode system. The axial displacement of an electrode upon heating was found to be sensitive to the depth to which it was initially dished. The displacement is also influenced by the radial clamping forces such as those produced by the electrode supports.

If warping of the screen electrode is calculated under these same conditions (i.e., temperature distribution) but for an initial dish depth of 0.040 in. (instead of 0.010 in.), a much larger axial displacement is found. In order to understand the complex dependence of axial displacement on initial depth, the axial displacement caused by heating to a given temperature distribution was calculated for electrodes with initial depths ranging from 0.004 in. to 4 in., with no mechanical loading present. The resulting curve is shown in Fig. 8. The appearance of a peak in the axial displacement curve was not expected. For large values of initial depth the curve is seen to approach a linear thermal expansion of about 0.002 in./in., which was expected in view of the final average electrode temperature of 375°C and expansion coefficient of 1.4×10^{-5}/°C. However, it was difficult to explain the decreasing portion of the curve (Fig. 8) because of the complicated nature of the two dimensional thermal stress problem being solved and because the competition between buckling forces is buried in the computer program. However, a satisfactory explanation of a qualitatively similar axial displacement vs initial position curve (e.g., with a peak) was found for an analogous, but more simple thermal buckling problem. We believe, therefore, that the behavior shown in Fig. 8 is real.

Secondly, the effect on warping of radially constraining an electrode which is thermally expanding was calculated by the stress analysis computer program. The case of the screen electrode expanding from 0.040-in. initial depth to a final depth of 0.062 in. was used. Without radial constraining forces the radial expansion of the electrode is 0.0125 in. In the subsequent calculations a radial boundary condition was included which held the radial expansion to values between 0.0124 and 0.0126 in. The radial constraint caused additional buckling of the electrode, as shown in Fig. 9. The curve

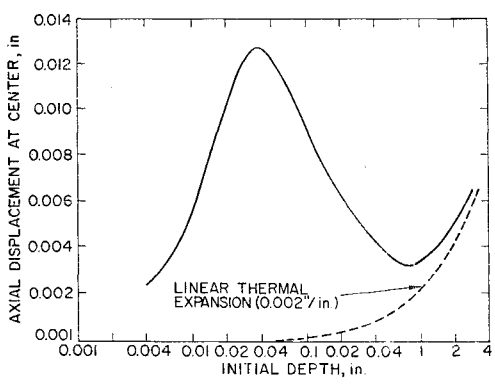

Fig. 8 Dependence of thermally induced axial displacement on initial axial position.

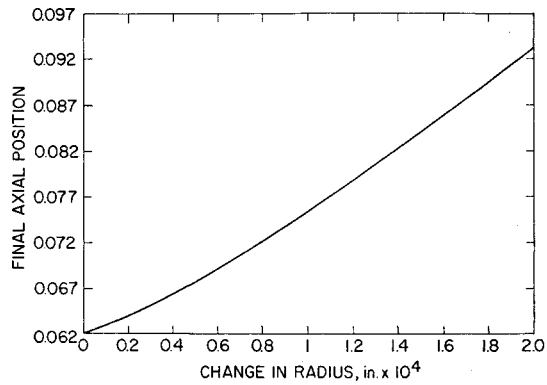

Fig. 9 Axial position of screen electrode center vs change in radius due to mechanical constraint.

gives the final axial position at the center of the electrode vs the difference between free radial expansion (0.126 in.) and the values specified by constraint. Thus, if clamping forces reduce radial expansion by 0.0001 in. the electrode center will move an additional 0.0135 in. (from 0.062 to 0.0755 in.). This high sensitivity of buckling to radial constraint was shown to be a basically geometric effect.

Ion Optics of Displaced Electrodes

In order to determine the change in the thrust vector due to the several perturbations of the ion engine, a digital computer was used to trace the ion trajectories and determine the thrust changes as the electrodes were moved. This computer program also allowed solution for the current flow rate from the plasma. These solutions were carried out for a single aperture of the accelerator system; the total effect was then obtained by summing over the many apertures with an appropriate current density weighting factor. The trajectories of the ions were determined by self-consistent solution for the fields, including the effects of space charge, for the given geometry.

The position of the ion source (upstream) plasma sheath was determined as part of each solution; this is a principal difference between this work and that of previous authors. It will be shown that the position and shape of the upstream sheath is quite important in determining the ion trajectories and current flow.

The downstream boundary, i.e., the position at which the beam becomes space-charge neutralized, was also determined. It was found, however, that the position and shape of this sheath was not sensitive to operating perturbations and in turn its position did not influence the trajectories or current to first order. A fixed position of downstream boundary was therefore used in all calculations.

The digital computer program used is a modification of one written by Hamza and Richley[3]; a similar program is described by Harrison.[4]

In the solution for the trajectories and upstream sheath position, the emitting source was divided into 13 annular segments; a self-consistent ion trajectory was started from each segment and traced through the accelerator region to the downstream boundary. If I_i is the current associated with the ith annular segment, the total axial thrust T_A from an aperture is

$$T_A \equiv k\Sigma I_i\,(V)^{1/2}\cos\phi_i \qquad (1)$$

where the summation is for all the trajectories, k is a constant, V = voltage difference between upstream and downstream plasma, and ϕ_i = angle between trajectory and axis at downstream boundary (exit angle).

The transverse thrust $T_\perp$ is given by a similar expression:

$$T_\perp \equiv k\Sigma I_i\,(V)^{1/2}\sin\phi_i \qquad (2)$$

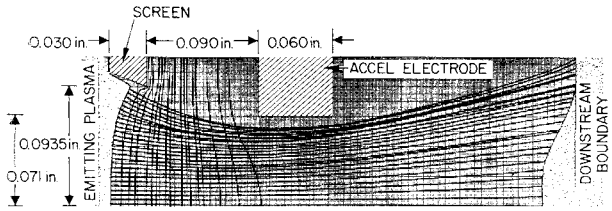

Fig. 10a Unperturbed engine configuration, case 1, Table 1.

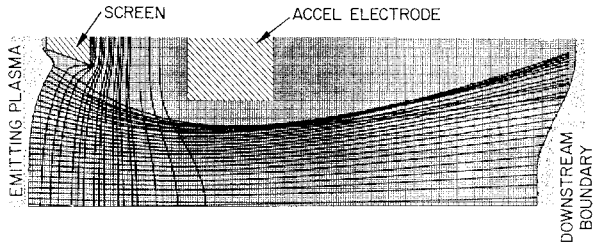

Fig. 10b Plasma boundaries and ion trajectories, case 2, Table 1.

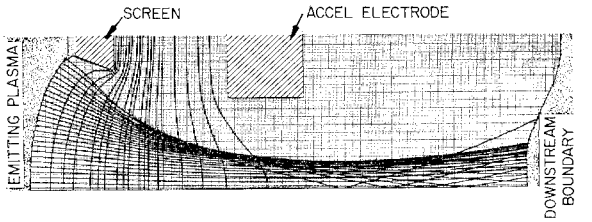

Fig. 10c Plasma boundaries and ion trajectories, case 4, Table 1.

because of axial symmetry, this summation leads to zero for an unperturbed electrode system.

It has been found that the major contribution to the change in thrust for axial displacements results from the movement of the upstream plasma boundary rather than from the change of direction of the trajectories downstream. A change in screen-accel electrode spacing causes the form and position of the boundary to change, resulting in a change in emitting area and hence in the total emitted current. The total current I_t passing through a single aperture can be expressed as

$$I_t = \sum_{0}^{A_s} \bar{j}_0 \, (\Delta A_i) \, F_i \qquad (3)$$

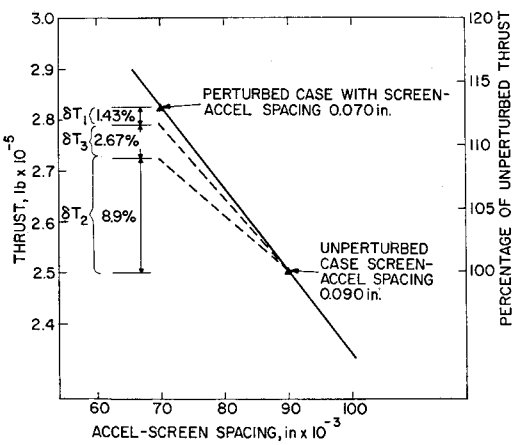

Fig. 11 Change in axial thrust with electrode spacing. δT_1 = change in axial thrust due to ion paths. δT_2 = change in axial thrust due to emitter area. δT_3 = change in axial thrust due to screen shielding.

Table 1 Electrode geometry of thruster

	Screen	Accelerator
Diameter, cm.	30	30
Thickness, in.	0.030	0.060
Open area, %	70	40
Hole diameter, in.	0.187	0.142
Hole spacing, in.	0.213	0.213
Material	Molybdenum	Molybdenum

where $\bar{j}_0$ is the density of current flowing through an element of area ΔA_i on the emitting surface, F_i is the "view factor" which accounts for the shielding effect of the screen electrode, A_s is the total curved surface area of the emitting plasma, and the summation is for all elements on the emitting surface. It can be seen that an increase in area A_s will cause an increase in total current and, hence, an increase in the thrust. The axial thrust from an aperture calculated from (1) can be expressed by means of (3) as

$$T = k(V)^{1/2} \Sigma \bar{j}_0 (\Delta A_i) \, F_i \cos\phi_i \qquad (4)$$

From (4) we can find the effect of small changes in the various parameters and write the change in thrust δT_A as

$$\delta T_A/T_A = \delta T_{1,A}/T_A + \delta T_{2,A}/T_A + \delta T_{3,A}/T_A + \delta T_{4,A}/T_A$$

where $\delta T_{1,A}$ = change in axial thrust due to change in ion paths alone, $\delta T_{3,A}$ = change in axial thrust due to change in emitting area, $\delta T_{3,A}$ = change in axial thrust due to change in screen electrode shielding, $\delta T_{4,A}$ = the change in thrust due to the change in ion arrival rate.

The axisymmetric electrode displacements and the changes in ion flow rate which were analyzed are listed in Table 2. From this table can be seen the relative magnitudes of the four differential terms listed above. Figure 10a, b, and c are computer drawings of the profiles of the plasma sheaths and of representative ion trajectories corresponding to cases 1, 2, and 4 of Table 1. Case I (Fig. 10a) represents the "nominal" unperturbed case and case 2 (Fig. 10a) the flow when the screen-accelerator electrode spacing is decreased. It is of interest to note that the total current through the aperture has increased because of the increase in the area of the emitting sheath that must retreat into the plasma to satisfy the boundary conditions. Inspection of the table shows that this effect alone is primarily responsible for the computed change in thrust. Case 3 shows the effect of approximately halving the flow rate in the nominal geometry. Case 4 (Fig. 10a) deals with a still further decrease in flow rate to about one quarter of the nominal value, and case 5 shows the effect of a subsequent decrease in electrode spacing. As the table shows, the axial thrust is most affected by the change in the ion flow due to the change in area of the sheath and to a much lesser extent by any perturbation to the trajectories. Of incidental interest is the striking change in trajectories shown in Fig. 10a as the sheath has retreated so that the focus

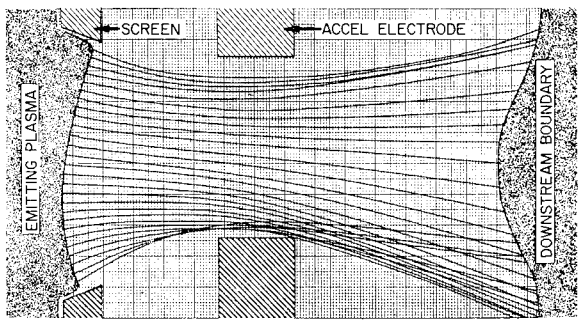

Fig. 12 Plasma boundaries and ion trajectories for the conditions of case 7 in Table 2.

Table 2 Effect of axially symmetric perturbations

Case no.	Screen-accel spacing, in.	Total ion current, ma	Axial thrust, μlb	$\delta T_A/T_A$, %	$\delta T_{1,A}/T_A$, %	$\delta T_{2,A}T_A$, %	$\delta T_{3,A}/T_A$, %	$\delta T_{4,A}/T_A$, %
1	0.090	1.32	25.03	...	...	...	...	...
2	0.070	1.49	28.29	13	1.43	8.9	2.67	...
3	0.090	0.753	15.02	−40	2.96	8.6	2.7	−54.3
4	0.090	0.382	8.21	...	...	...	...	...
5	0.070	0.429	8.87	8.0	3.4	4.5	0.1	...

Table 3 Changes in thrust due to movement of the accel electrode

Case no.	Screen-accel spacing, in.	Total ion, current, ma	Transverse displacement of accel, in.	$\overline{\delta\phi_i}$ Average deflection, deg.	Axial thrust, lb $\times 10^{-6}$	Transverse thrust, lb $\times 10^{-6}$	Rotation of thrust vector, deg.
6	0.090	1.34	0.0071	4.13	24.87	1.278	2.94
7	0.090	1.35	0.0142	8.20	24.72	2.529	5.84
8	0.090	0.388	0.0071	4.49	8.12	0.357	2.52
9	0.090	0.391	0.0142	8.80	8.03	0.708	5.04

electrode causes the ions to be strongly converged into a narrow beam. The change in thrust due to an axial displacement of the accel electrode is illustrated graphically in Fig. 10b. Within the limit of the approximation of linearity, the coefficient is 0.65%/mil spacing change.

Transverse electrode movements were analyzed by a suitable superposition of axially symmetric and planar solutions. The planar solutions used values of arrival rate corresponding to the axially symmetric cases 1 and 4 (Table 1). The electrode perturbations introduced were transverse displacements of the accel electrode of 0.0071 in. and 0.0142 in. The results are summarized in Table 3; Fig. 10c shows the computed trajectories for case 7 of Table 2 and Fig. 11 plots the angular deflection as a function of transverse displacement. A self-consistent boundary was found in each case. Inspection of Fig. 12 shows that the beam is deflected in the opposite direction to the electrode displacement and that the two beam edges are moved in this direction by approximately equal amounts. The deflection of the beam in the opposite direction of the electrode motion may be surprising at first glance. This behavior results from the distortion of the electric fields by the motion of the accel aperture relative to the focus electrode hole. The transverse components of field so created are strongest on that portion of the accel aperture nearest the axis; these fields deflects the ions in the opposite direction.

In Table 3 and Fig. 11 the average trajectory deflection ($\overline{\delta\phi_i}$) represents the change in direction of the trajectories, evaluated at the downstream boundary, from the unperturbed to the perturbed state. This term is evaluated in the plane of the motion of the electrode and therefore represents the maximum deflection. In order to evaluate the transverse thrust for the entire beam, it was assumed that the transverse thrust component varied as the sine of the azimuthal angle around the beam axis. The summation of these transverse components is shown in the table, together with the equivalent angle of rotation of the thrust vector (T_T/T_A). Figure 13 also presents the results of Lathem.[1] This relatively small difference can be explained by a number of factors. The geometry and voltages assumed in this study are somewhat different. Thus, the lens produced in this study geometry is slightly stronger, which tends to reduce the divergence; in previous work no account was taken of the relocation of the emitting plasma caused by the electrode perturbation. In addition, although it is a small effect, Lathem did not determine the correct position of the downstream boundary.

In consideration of the third type of electrode misalignment (i.e., tilt), as shown in Fig. 2c, it can be noted that for a typical thruster with a diameter of 12 in. and a nominal spacing between the screen and accelerator electrode of 0.090 in., the maximum angle for gross tilt of the entire accel electrode is of the order of $\tan^{-1} 0.015$ assuming the electrodes to be touching at the center and spaced 0.090 in. at the edges. This is equivalent to an angle of about 0.8°. (However, localized warping could increase the angle to some extent.) A case has been run with symmetric tilt of 1.5° about the unperturbed center line. This produces a maximum displacement of the accel electrode of 0.002 in. The results from the run show no significant change in ion optics or emission density.

However, tilt may be a significant factor at the center of the engine where the displacement of the accel electrode can be regarded as a combination of an axial movement and a tilt. In this case a satisfactory solution can be found by considering the appropriate axial displacement alone.

The values of the coefficients relating the effects of perturbations to their causes are summarized in Table 4. These values are used together with the calculated magnitudes of electrode displacement, to provide the estimated total thrust vector variation of a single thruster.

The rate of change in axial thrust with axial spacing of the electrodes at constant ion arrival rate is given by $\alpha|_P$ for two values of perveance P. The rate of change of axial thrust from a single aperture with emitted ion current at a nominal perveance P is given by $\beta|_P$. Similarly, the rate of change of transverse thrust of a single aperture and rotation of the thrust vector with transverse displacement of the accel electrode are given by $\eta|_P$ and $\omega|_P$, respectively.

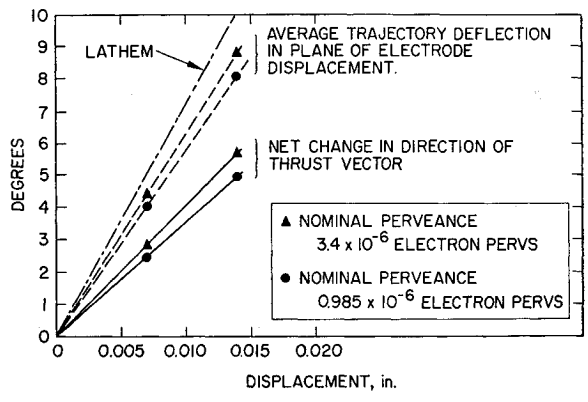

Fig. 13 Angular deflection as a function of transverse displacement.

Table 4 Parameters defining change in thrust vector for various perturbations

P (Nominal perveance), electron pervs	$\alpha\|_P$, lb/0.001 in.	$\beta\|_P$, lb/mA	$\gamma\|_P$, lb/0.001 in.	η'_P, lb/0.001 in.	$\omega\|_P$, deg/0.001 in.
3.4×10^{-6}	-1.63×10^{-7}	1.765×10^{-5}	2.18×10^{-8}	-1.78×10^{-7}	0.411
0.985×10^{-6}	-0.33×10^{-7}	0.684×10^{-5}	1.26×10^{-8}	-0.498×10^{-7}	0.354

Conclusions

Several ways have been discussed in which the thrust of an electron bombardment engine can alter so as to have a transverse component. Four causes of thrust perturbation have been considered; changes in flow rate, changes in axial spacing of the electrodes, transverse misalignment, and tilt between the electrodes. It has been shown that significant geometric changes arise from the bowing of the accel and screen electrodes due to heat radiated from the discharge chamber and due to beam interception.

The effect of the perturbations on the ion flow was calculated for a single aperture in the accelerator system. It was found that changes in ion flow rate produce a nearly comparable percentage change in the axial thrust. Axial changes in electrode spacing produce a thrust change which depends on the operating level and is higher at the higher flow rates.

In the case of transverse displacements, the changes in ion flow rate due to sheath movement are negligible and the change in thrust is due to the geometric changes of the trajectories. Tilt of the electrodes that is not accompanied by a translation of the electrodes produces a negligible effect under conditions which are likely to be encountered. Those perturbations which are of significance were expressed by linear coefficients relating the change in axial or transverse thrust to electrode displacement.

The magnitude of the mechanical deformations and the resulting perturbations in ion flow have been calculated for a typical 30-cm Kaufman thruster operating at a nominal thrust of 30 mlb. It was found that a tolerance of 0.002 in. in axial spacing of the two electrodes (due to assembly errors for instance) produces a 1.3% variation in the total axial thrust. Whereas an uncertainty of 0.010 in. in relative transverse positions of the electrodes results in a 4° uncertainty in the resultant thrust vector. Rotation of the electrodes with respect to each other produces a rotational torque and a second order reduction in axial thrust. Thus, a 1° rotation causes a roll axis torque of 4.32×10^{-3} in.-lb and a less than 1% decrease in axial thrust.

References

[1] Lathem, W. C., "Effects of Electrode Misalignment in Kaufman Thrusters," *Journal of Spacecraft and Rockets*, Vol. 5, No. 6, June, 1968, pp. 735–737.

[2] O'Donnel, W. J. and Langer, B. F., "Design of Perforated Plates," *Journal of American Society of Mechanical Engineers*, Vol. 30, 1962, pp. 307–320.

[3] Hamza, V. and Richley, E. A., "NASA Rep. TND-1323," Washington, D.C., 1962: Rept. TND-1714, 1963, NASA.

[4] Harrison, J. L., "A Digital Computer Program for Computing Ion-Saturation Currents from A Plasma of Uniform Density In A Two-Dimensional Geometry," *Journal of Applied Physics*, Vol. 30, 1968, p. 3827.